JOURNAL OF CATALYSIS **178,** 284–298 (1998)
ARTICLE NO. CA982151

Silica Hybrid Gel Catalysts Containing Group(VIII) Transition Metal Complexes: Preparation, Structural, and Catalytic Properties in the Synthesis of *N,N*-Dimethylformamide and Methyl Formate from Supercritical Carbon Dioxide

Oliver Kröcher,* René A. Köppel,* Michael Fröba,† and Alfons Baiker*,[1]

*Laboratory of Technical Chemistry, Swiss Federal Institute of Technology, ETH Zentrum, CH-8092 Zürich, Switzerland; and †Institute for Inorganic and Applied Chemistry, Universität Hamburg, D-20146 Hamburg, Germany

Received February 16, 1998; revised May 12, 1998; accepted May 12, 1998

Sol-gel derived hybrid materials containing group(VIII) transition metal complexes in a porous silica network were prepared and tested for the catalytic synthesis of *N,N*-dimethylformamide (dmf) and methyl formate (mf) from supercritical carbon dioxide, hydrogen, and dimethylamine and methanol/triethylamine, respectively. Bifunctional silylether phosphines $X = Ph_2P(CH_2)_2Si(OEt)_3$ and $Y = Me_2P(CH_2)_2Si(OEt)_3$ were used as ligands for the preparation of complexes of the type $RuCl_2X_3$, $RuCl_2Y_3$, $MClX_3$ (M = Ir, Rh), and MCl_2X_2 (M = Pt, Pd). The silylether complexes were anchored in a silica matrix by co-condensation with $Si(OEt)_4$. The textural and structural properties of the hybrid gels were characterized by means of ^{31}P and ^{29}Si NMR spectroscopy, extended X-ray absorption fine structure (EXAFS), X-ray diffraction (XRD), transmission electron microscopy (TEM), and nitrogen and argon physisorption. ^{31}P NMR spectroscopy confirmed nondestructive immobilization of the Ru, Pt, Pd, Rh, and Ir complexes. TEM and XRD analyses proved the homogeneity and noncrystallinity of the materials. The degree of condensation of the gels and the molecular mixing of the components has been investigated by solid state ^{29}Si NMR spectroscopy. Textural characterization showed that all gels were micro- to mesoporous. EXAFS measurements indicated no metal–metal interactions, confirming that the organometallic complexes were immobilized as monomers. From all catalysts silica matrix stabilized ruthenium complexes exhibited highest activities at 100% selectivity in dmf synthesis from CO_2, H_2, and dimethylamine. The corresponding turnover frequency (TOF) of 1860 h^{-1} exceeded those reported so far for heterogeneous catalysts by a factor of 600. In methyl formate synthesis, TOFs up to 115 h^{-1} were reached.

INTRODUCTION

Based on its large-scale availability, CO_2 represents a suitable starting material for the production of valuable fuels and chemicals (1–7). In the past decades the synthesis of *N,N*-dimethylformamide (dmf) and methyl formate (mf) from carbon dioxide has gained considerable attention as an interesting alternative route for producing these basic chemicals (6–20). Both reactions are exothermic but, depending on the reaction conditions, neutral or slightly exergonic due to the unfavorable entropy change. To reach high product yields, high pressures and relatively low temperatures have to be applied. In order to stabilize the formic acid, which is regarded as a crucial intermediate, the addition of a basic additive is beneficial. In mf synthesis the stabilizing additive is a tertiary amine such as triethylamine. In dmf synthesis dimethylamine acts as a basic additive and as reactant, forming the product on reacting with the formic acid intermediate. To reach high reaction rates, the use of a catalyst is crucial for this type of reactions.

Various group(VIII) based transition metal complexes have been tested as catalysts in the synthesis of dmf and mf from CO_2 in liquid solvents (1, 6–14). Rhodium, iridium, and ruthenium based systems with phosphine ligands proved to be most effective for dmf synthesis (1, 8, 10). However, overall catalytic activity remained low. Similar to dmf synthesis, phosphine complexes of group(VIII) transition metals with basic co-catalysts were found to be active homogeneous catalysts for the formation of methyl formate from CO_2, H_2, and methanol in the presence of organic solvents (1, 9, 13).

A substantially more efficient reaction system for dmf and mf synthesis, not requiring any additional solvent, was recently reported by Jessop *et al.* (6, 15–17), making use of a supercritical phase of carbon dioxide ($scCO_2$) and hydrogen, in which the $[RuCl_2(P(Me)_3)_4]$ catalyst is dissolved. In this case $scCO_2$ serves as both a reactant and a solvent. The high reaction rate was attributed to favorable mass transfer effects, high solubility of H_2, and weak solvation of the catalyst compared to liquid solvents (16, 21). The application of complexes soluble in $scCO_2$ was reported to be crucial for achieving high activities in this reaction system.

[1] To whom correspondence should be addressed. E-mail: baiker@tech.chem.ethz.ch.

0021-9517/98 $25.00

However, the use of homogeneous catalysts has often limited technical utility on a large scale, owing to difficulties in catalyst separation and recovery. On the other hand, known heterogeneous catalysts exhibited only low activity for the synthesis of dmf (11, 22).

An interesting design strategy is the heterogenization of homogeneous transition metal complexes, resulting in materials which combine the activity, selectivity, and accessibility of specially tailored metal centers in homogeneous catalysts with the technical advantages of heterogeneous catalysts. Early attempts to immobilize catalytically active complexes were directed to anchor complexes to organic polymers or inorganic supports (23–26). Among the supports used, silica has gained much attention due to the ease of functionalization through its surface OH-groups and its rigid structure. To surface-attach complexes, mostly bifunctional silylether phosphines were bonded with the phosphine site to the metal center and the silylether site to free hydroxy groups on the surface of silica. Inherent problems with catalysts obtained by this route are leaching of the active component under operating conditions and low surface loading (25, 26).

In the past few years, anchoring of catalytically active transition metal complexes via organic groups within oxide networks (mainly silica) by a modified sol-gel process has received considerable attention as a method to overcome these problems (25–29). Silica gel-like metal-containing materials with highly active tailored metal centers can be produced by simultaneous cocondensation of transition metal silylether complexes with tetraalkoxysilane according to:

$$n\,Si(OEt)_4 + m\,R\text{-}Si(OEt)_3 + (4n+3m)\,H_2O \xrightarrow{H^+} n\,Si(OH)_4 + m\,R\text{-}Si(OH)_3 + (4n+3m)\,EtOH \quad [1]$$

$$n\,Si(OH)_4 + m\,R\text{-}Si(OH)_3 \xrightarrow{H^+} (SiO_2)_n(R\text{-}SiO_2)_m + (2n+3/2m)\,H_2O. \quad [2]$$

The catalysts produced are often as active as their homogeneous analogues because organometallic complexes are incorporated unchanged within a porous matrix which allows accessing the catalytically active centers. Moreover, the immobilized complexes are generally more stable towards oxygen and water, compared to their free analogues and show negligible leaching.

The aim of the present work was to tailor sol-gel derived catalysts for the synthesis of *N,N*-dimethylformamide and methyl formate from carbon dioxide, hydrogen, and dimethylamine or methanol/triethylamine, respectively, without additional solvents. In a preliminary study (18) we have recently shown that sol-gel derived hybrid catalysts exhibit interesting properties for the synthesis of dmf. Here, we report the preparation and structural characterization of these functionalized silica materials and their catalytic behavior in the synthesis of dmf and mf.

EXPERIMENTAL

Materials

All preparations were carried out under dry, oxygen-free argon using Schlenk techniques unless stated otherwise. Solvents were used in spectrophotometric purity, dried over molecular sieve, degassed, and stored under argon. Vinyltriethoxysilane was supplied from Alfa and diphenylphosphine from Strem Chemicals. All other compounds were supplied from Fluka. Dimethylphoshine was prepared as described in the literature (30).

Silylether phosphine ligands. (Trisethoxysilyl)ethyldiphenylphosphine (**1**) was prepared by photochemical reaction of vinyltriethoxysilane (20.2 g, 106 mmol) and diphenylphosphine (19.8 g, 106 mmol) for 4 days and purified by distillation (1 Torr, 174°C) to give a colorless liquid (31), (**1**, 38.7 g, 97%): ^{1}H NMR ($CDCl_3$) δ 7.2–7.7 (m, 10 H, ArH), 3.80 [q, $J = 7.0$ Hz, 6 H, OCH_2CH_3], 2.13 (m, 2 H, CH_2P), 1.21 [t, 9 H, $J = 7.0$ Hz, OCH_2CH_3], 0.72 (m, 2 H, $SiCH_2$); $^{31}P\{^1H\}$ NMR ($CDCl_3$) δ −8.4.

(Trisethoxysilyl)ethyldimethylphosphine (**2**) was prepared by the reaction of vinyltriethoxysilane (13.1 g, 68.7 mmol) and dimethylphosphine (4.27 g, 68.7 mmol) according to literature (31). Fractional distillation gave a colorless liquid (0.8 Torr, 61–63°C), (**2**, 16.0 g, 92%): ^{1}H NMR ($CDCl_3$) δ 3.83 [q, $J = 7.0$ Hz, 6 H, OCH_2CH_3], 1.41 (m, 2 H, CH_2P), 1.23 [t, $J = 7.0$ Hz, 9 H, OCH_2CH_3], 0.99 [d, $^2J(HP) = 1.8$ Hz, 6 H, PCH_3], 0.69 (m, 2 H, $SiCH_2$); $^{13}C\{^1H\}$ NMR ($CDCl_3$) δ 58.6, 23.9 (d, $^1J(CP) = 10.5$ Hz, 1 C, CH_2P), 18.2, 13.4 [d, $^1J(CP) = 13.5$ Hz, 2 C, $P(CH_3)_2$], 5.5 [d, $^1J(CSi) = 9.2$ Hz, 1 C, $SiCH_2$]. ^{31}P NMR ($CDCl_3$): $\delta = -44.1$.

Hybrid gel precursors. Structural formula of the different precursor complexes are summarized in Scheme 1. $RuCl_2\{PPh_2(CH_2)_2Si(OEt)_3\}_3$ (**3**) was prepared according to the literature (32). $RuCl_3 \cdot xH_2O$ (0.60 g, 2.30 mmol) was dissolved in methanol (75 ml) in a Schlenk tube and **1** (5.18 g, 13.8 mmol) was added under stirring. Sodium borohydride was added in small portions until the color changed to brown. After further stirring for 15 h methanol was evaporated (15 h, 60°C, 0.5 Torr). The solid residue was shaken 30 min with CH_2Cl_2 (50 ml) and the insoluble salts subsequently filtered off over Celite. Finally the CH_2Cl_2 was evaporated at 50°C (15 h, 0.5 Torr) and the oily residue extracted two times with pentane, (**3**, 5.93 g, 89%): Anal. Calcd for $C_{60}H_{87}O_9Cl_2P_3RuSi_3$: C, 55.37; H, 6.74. Found: C, 55.08; H, 6.46.

$RuCl_2\{PMe_2(CH_2)_2Si(OEt)_3\}_3$ (**4**). The preparation was carried out analogously to the preparation of **3** using **2** as a ligand. The color of the solution changed to yellow–brown after the addition of sodium borohydride, (**4**, 2.37 g, 68%).

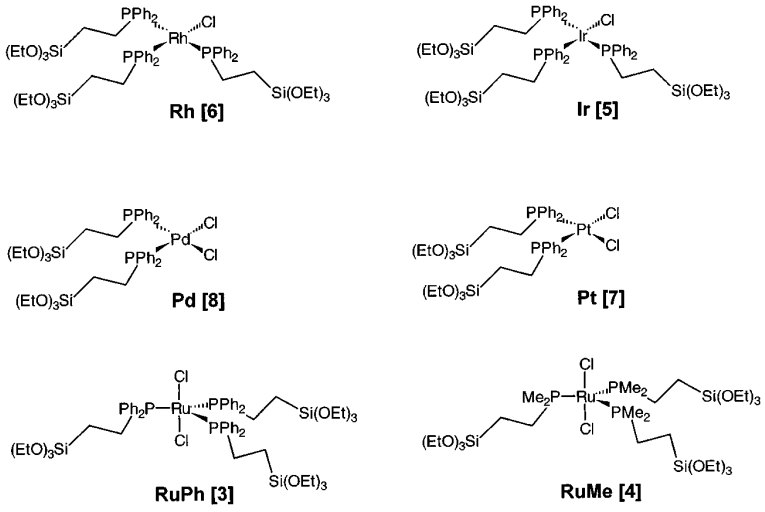

SCHEME 1. Structural formula and denotations of group(VIII)-metal silylether complexes used as precursors for hybrid gel catalysts. Note that structural formula of complexes **[3]** and **[4]** have not been fully confirmed (see text).

$IrCl\{PPh_2(CH_2)_2Si(OEt)_3\}_3$ (**5**). $[IrCl(COD)]_2$ (COD = 1,5-cyclooctadiene) (0.491 g, 0.731 mmol) was dissolved in toluene (10 ml) in a Schlenk tube and **1** (1.92 g, 5.10 mmol) in toluene (10 ml) was added dropwise under stirring. The solution was stirred for 3 h, during which the color changed from red to orange. Toluene was evaporated (60°C, 0.1 Torr) and the viscous residue was dissolved in hexane (25 ml). After cooling to −20°C a red-orange oil was obtained which was dried at 60°C and 0.1 Torr. The mother liquor was concentrated and cooled again, (**5**, 1.61 g, 81%): $^{31}P\{^1H\}$ NMR (C_6D_6) δ −1.8 [t, $^2J(PP) = 14.1$ Hz, 1 P], −13.0 [d, $^2J(PP) = 13.6$ Hz, 2 P]. Anal. Calcd for $C_{60}H_{87}ClO_9P_3IrSi$: C, 53.10; H, 6.46; P, 6.85. Found: C, 53.27; H, 6.66; P, 7.14.

$RhCl\{PPh_2(CH_2)_2Si(OEt)_3\}_3$ (**6**) was prepared analogously to **5**, except that $[RhCl(COD)]_2$ (0.542 g, 1.10 mmol) and **1** (2.60 g, 7.17 mmol) was used. The color changed from red-orange to red during the reaction, (**6**, 1.99 g, 71%): $^{31}P\{^1H\}$ NMR (C_6D_6) δ 46.9 [dt, $^2J(PP) = 39.5$ Hz, $^1J(PRh) = 187.9$ Hz, 1 P], 30.6 [dd, $^2J(PP) = 39.4$ Hz, $^1J(PRh) = 139.2$ Hz, 2 P]. Anal. Calcd for $C_{60}H_{87}ClO_9P_3RhSi$: C, 56.84; H, 6.92; P, 7.33; Rh, 8.12. Found: C, 57.12; H, 6.76; P, 7.34; Rh, 8.27.

cis-$PtCl_2\{PPh_2(CH_2)_2Si(OEt)_3\}_2$ (**7**). To a suspension of $PtCl_2(COD)$ (0.997 g, 2.66 mmol) in toluene (20 ml) **1** (2.10 g, 5.58 mmol) was added dropwise. A yellow-greenish solution was formed which was concentrated to 5 ml. After the addition of pentane a white precipitate fell out which was washed thoroughly with pentane, (7, 2.39 g, 88%): ^1H NMR ($CDCl_3$) δ 7.1–7.5 (m, 20 H, ArH), 3.64 (q, $J = 7.0$ Hz, 12 H), 2.40 (m, CH_2P, 4 H), 1.08 (t, $J = 7.0$ Hz, 18 H), 0.72 (m, 4 H, $SiCH_2$). $^{31}P\{^1H\}$ NMR ($CDCl_3$) δ 11.8 [*pseudo*-t, $^1J(PPt) = 3655$ Hz, 2P].

cis-/trans-$PdCl_2\{PPh_2(CH_2)_2Si(OEt)_3\}_2$ (**8**). $PdCl_2(COD)$ (1.01 g, 3.54 mmol) was suspended in toluene (25 ml) and **1** (2.70 g, 7.17 mmol) was added dropwise. A clear orange solution was formed which was worked up as described for **7**, (**8**, 3.10 g, 94%): ^1H NMR ($CDCl_3$) δ 7.2–7.5, 7.6–7.7 (2m, 20 H, ArH), 3.71 (q, $J = 7.0$ Hz, 12 H), 2.47 (m, 4 H, CH_2P), 1.13 (t, $J = 7.0$ Hz, 18 H), 0.79 (m, 4 H, $SiCH_2$). $^{31}P\{^1H\}$ NMR ($CDCl_3$) δ 32.3 (*cis*), 22.0 (*trans*). Anal. Calcd for $C_{40}H_{58}Cl_2O_6P_2PdSi_2$: C, 51.64; H, 6.28; Cl, 7.62. Found: C, 51.57; H, 6.25; Cl, 7.92.

Sol-gel derived catalysts. For all acid-catalyzed sol-gel preparations a 1.5l flat-bottom three-neck flask equipped with an argon inlet and a bubble gauge was used. Scheme 2 illustrates the main features of the incorporation of the

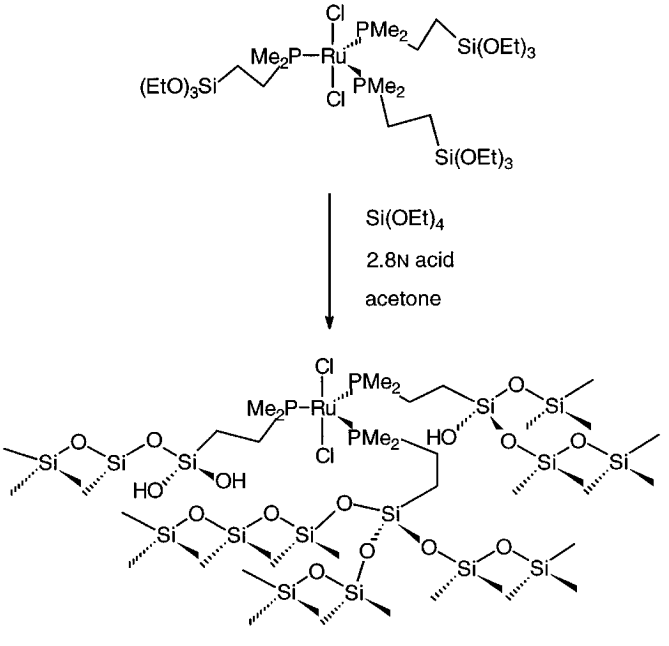

SCHEME 2. Reaction scheme illustrating the incorporation of $RuCl_2\{PMe_2(CH_2)_2Si(OEt)_3\}_3$ into the silica matrix using a sol-gel process.

metal silylether complexes at the example of RuMe complex (Scheme 1). Appropriate amounts of tetraethoxysilane (TEOS) and the complexes were dissolved under argon in such an amount of acetone that no precipitation occurred after addition of the acid. The amount of acid was calculated to get a sevenfold excess of the stoichiometric equivalent of water necessary for the complete hydrolysis of the ethoxysilyl groups. 2.8 *N* acetic acid or orthophosphoric acid was used. The flask was stoppered and the solution was moderately stirred for 24 h. Then a continuous flow of argon was passed through the flask for 3 days. During this time acetone evaporated off and glassy colored lumps remained, which had the same color as the precursor complex. The solid was kept for further 4 days in an open beaker. The lumps were crushed with a mortar and washed three times with water (20 ml) and three times with acetone (20 ml). The solid was dried for 6 h at room temperature under vacuum (0.1 Torr).

In a typical experiment **7** (0.713 g, 0.70 mmol) and tetraethoxysilane (7.29 g, 7.82 ml, 35.0 mmol, 50 eq.) were dissolved in acetone (80 ml) and orthophosphoric acid (18.2 ml) was added. Yield: 2.83 g of white RuMe-1. Throughout the article a set of acronyms (Table 1) is used for the individual hybrid gels.

Physicochemical Characterization

Elemental analyses of the prepared compounds were carried out on a LECO CHN-900. Phosphorus contents were determined with $Pb(ClO_4)_2$, and chlorine, by titration with $AgClO_4$ solution. Metal contents were determined by ICP-AES.

For obtaining ^{1}H NMR spectra, a Bruker DPX 300 instrument was used (sweep frequency 300 MHz, internal standard TMS). Multiplicities are abbreviated by s = singlet, d = doublet, t = triplet, and q = quadruplet. ^{31}P NMR spectra of liquids were recorded on a Bruker AMX 400 at a sweep frequency of 162.0 MHz and using 85% orthophosphoric acid as external standard. ^{31}P NMR spectra of solids, applying the cross-polarization magic-angle-spinning (CP/MAS) technique, were measured at a sweep frequency of 162.0 MHz, using 85% orthophosphoric acid as external standard. Single-pulse-excitation (SPE) and CP/MAS ^{29}Si NMR measurements were made with a Bruker AMX 400 at 79.5 MHz, applying TMS as an internal standard. The sample size was about 500 mg for solid state NMR spectroscopy. Magic-angle-spinning was routinely carried out at 4 kHz spinning rate. The number of scans was 2048 for CP/MAS measurements and at minimum 64 for SPE experiments. The repetition time for CP/MAS experiments was about 4 s and 200 s for SPE. Chemical shifts are reported in δ-units. $T_{1\rho H}$ was measured via ^{29}Si with a separate experiment described by Schaefer *et al.* (33). Peak deconvolution and evaluation of the spectra were accomplished with the standard software 1D WINNMR from Bruker. Measurements were performed at 300 K.

For transmission electron microscopic (TEM) measurements, samples were suspended in abs. ethanol, treated with ultrasound and applied to a carbon carrier foil. All investigations were carried out with a Philips CM30ST operated at 300 kV (LaB_6, Ko-Ap 3, d = 50 μm, single tilt holder).

X-ray powder diffraction (XRD) patterns were measured on a Siemens Θ/Θ D5000 powder X-ray diffractometer. The diffractograms were recorded with CuKα radiation over a 2Θ range of 10° to 80° using a position-sensitive detector with Ni-filter.

The specific surface areas (S_{BET}) and mean pore diameters ($\bar{d}_{N2}$) were determined from nitrogen physisorption at 77 K using a Micromeritics ASAP 2010 instrument. Prior to measurement, the samples were degassed to 0.1 Pa at 403 K. S_{BET} were calculated in a relative pressure range 0.05–0.2 assuming a cross-sectional area of 0.162 nm^2 for the nitrogen

TABLE 1

Textural Properties of Hybrid Gel Catalysts

Catalyst	Complex		Complex : TEOS	Acid	Metal cont./wt%	Physisorption: N_2		Physisorption: Ar	
						S_{BET}/m^2 g^{-1} [a]	$\bar{d}(N_2)$/nm [b]	S_{micro}/m^2 g^{-1} [c]	$\bar{d}$(Ar)/nm [d]
Si	—		0 : 100	H_3PO_4	0	880	3.2	—	—
RuPh-1	$RuCl_2\{PPh_2(CH_2)_2Si(OEt)_3\}_3$	**3**	1 : 50	H_3PO_4	1.7	460	2.8	—	—
RuPh-2	$RuCl_2\{PPh_2(CH_2)_2Si(OEt)_3\}_3$	**3**	1 : 20	H_3PO_4	2.8	200	3.4	130	2.1
RuMe-1	$RuCl_2\{PMe_2(CH_2)_2Si(OEt)_3\}_3$	**4**	1 : 50	H_3PO_4	1.9	510	2.3	290	2.0
RuMe-2	$RuCl_2\{PMe_2(CH_2)_2Si(OEt)_3\}_3$	**4**	1 : 20	H_3PO_4	3.7	<5	—	—	—
RuMe-3	$RuCl_2\{PMe_2(CH_2)_2Si(OEt)_3\}_3$	**4**	1 : 20	$MeCO_2H$	3.9	70	3.4	30	2.1
Ir	$IrCl\{PPh_2(CH_2)_2Si(OEt)_3\}_3$,	**5**	1 : 50	$MeCO_2H$	3.7	480	2.1	310	1.8
Rh	$RhCl\{PPh_2(CH_2)_2Si(OEt)_3\}_3$	**6**	1 : 50	$MeCO_2H$	2.0	800	2.4	360	2.0
Pt	$PtCl_2\{PPh_2(CH_2)_2Si(OEt)_3\}_2$	**7**	1 : 50	H_3PO_4	4.8	770	4.1	—	—
Pd	$PdCl_2\{PPh_2(CH_2)_2Si(OEt)_3\}_2$	**8**	1 : 50	$MeCO_2H$	2.5	430	2.3	210	1.8

[a] BET surface area.
[b] Mean pore diameter.
[c] Mircropore surface area determined from argon physisorption.
[d] Mean pore diameter from argon physisorption.

molecule. The pore size distributions were calculated applying the Barrett–Joyner–Halenda (BJH) method (34) to the desorption branch of the isotherms (35). The occurrence of microporosity could be estimated from t-plot constructions (36). Argon physisorption measurements were carried out at 77 K on the same instrument to determine the micropore surface area (S_{micro}) and the mean pore diameter ($\bar{d}_{Ar}$), applying Dubinin–Astakhov calculations (37).

The extended X-ray absorption fine structure (EXAFS) spectra were recorded at the storage ring DORIS III (HASYLAB@DESY, Hamburg, Germany) at the RÖMOII beam line which was equipped with a Si (311) double-crystal monochromator. In order to reduce contributions from higher harmonics, the second monochromator crystal was detuned to 50% of the maximum intensity. The slit before the monochromator, as well as that in front of the first ion chamber, was set to 1 mm height. The spectra of the L_{III} absorption edges (Ir L_{III} and Pt L_{III}) were calibrated against the first inflection point of the Pt L_{III} edge (11564 eV) of a Pt foil which was measured simultaneously. In case of the metal K edges (Ru, Rh, and Pd) the spectra were calibrated against the first inflection point of the Pd K edge (24,350 eV) of a Pd metal foil. All spectra were recorded in a transmission mode at room temperature using a continuous scan technique (QEXAFS) (38). For the L_{III} edges the counting time per data point was 0.7 s linked with a distance between data points of 2 eV, whereas the K edges were recorded with 0.5–0.6 s per data point and distances of 3–4 eV. All samples were prepared as pressed polyethylene pellets in which the metal content was adjusted to yield an absorption jump $\Delta\mu$ of about 0.3–0.5 at the respective absorption edge. For further data analysis the program WinXas (39) was used. Theoretical calculations of the phase shifts and back scattering amplitudes were calculated using FEFF6.01 (40).

Catalytic Tests

Catalytic tests for the synthesis of dmf and mf were carried out in a 500 ml stainless-steel autoclave agitated by a straight 6-blade turbine. In a typical experiment for dmf synthesis the autoclave containing 5×10^{-5} mol catalyst was flushed with carbon dioxide, charged with liquid dimethylamine (0.71 mol), pressurized with hydrogen (4 MPa), and heated up to 373 K at a stirring rate of 300 min^{-1}. After thermal equilibration hydrogen was pressed into the reactor (8.5 MPa) and then carbon dioxide (13.0 MPa) was added to start the reaction. The reaction time was typically 15 h. After the reaction, the autoclave was cooled rapidly, vented, and opened. The catalysts were filtered off using a syringe filter (0.2 μm). For the production of methyl formate, methanol and triethylamine was charged instead of dimethylamine.

Product analysis was performed using a gas chromatograph (Hewlett Packard) equipped with a thermal conductivity detector. Gaseous compounds were separated on a Porapak QS column (5 m, 1/8 in. OD, 80–100 mesh) and liquid products on a Supelco SPB-1 fused silica capillary column (60 m, 0.53 mm ID, 5 μm film).

Hydrogen, dimethylamine, and carbon dioxide were purchased from Pangas, methanol (analytic purity) from Riedel-de-Haën, and triethylamine (anhydrous, purum) from Siegfried Company. Prior to all tests the reactor was carefully cleaned with ethanol. Blank experiments were carried out regularly to confirm that no catalytically active material remained in the reactor after cleaning. For further experimental details see Ref. (41).

RESULTS

Hybrid Gel Precursors

For the immobilization of organometallic complexes in a silica matrix silylether complexes of group(VIII) transition metals have been prepared. Ligand exchange of chloro COD complexes of Pd, Pt, Rh, and Ir with $Ph_2P(CH_2)_2Si(OEt)_3$ produced the corresponding hybrid gel precursors **5**, **6**, **7**, and **8** (Table 1) in good yields. The *cis*-configuration of **7** was confirmed by the $^1J(^{195}Pt, ^{31}P)$ value of 3655 Hz, which is typical for phosphines standing *trans* to chlorine in complexes of this type (42, 43), and by comparison with the NMR data of the related compound *cis*-$PtCl_2(PPh_2Et)_2$ (44). The reaction of $PdCl_2(COD)$ with $Ph_2P(CH_2)_2Si(OEt)_3$ gave **8** with a *cis/trans* ratio of 23 : 77. The typical down-field shift of the *cis*-configuration of phosphine groups in this type of compounds allowed us to assign the peaks in the ^{31}P NMR spectra (42–46).

In case of the ruthenium complexes, only partial ligand exchange could be achieved when starting from $[RuCl_2(COD)]_n$. Hence, a synthetic route from ruthenium chloride and $Ph_2P(CH_2)_2Si(OEt)_3$ (**1**) or $Me_2P(CH_2)_2Si(OEt)_3$ (**2**), respectively, with $NaBH_4$ as reductant was chosen. In contrast to the well defined precursors **5**, **6**, **7**, and **8**, characterization of the Ru precursors by NMR spectroscopy was troublesome. In all cases five or more signal groups were discerned in the ^{31}P NMR spectra, making assignment of the peaks difficult. In contrast to the utilization of simple phosphine ligands, the use of bifunctional silylether ligands prevented the formation and isolation of pure compounds. The main reasons were: (i) slightly altering reaction conditions led to various products which differed in the number of ligands or in the degree of dimerization, (ii) fluctual behavior of the ligands, (iii) cleavage of ligands in solution, and (iv) rearrangement reactions (47).

Sol-Gel Derived Catalysts

An overview on the hybrid gel catalysts prepared is given in Table 1. Among various methods tested for sol-gel processing of the silylether complexes, a procedure similar to

TABLE 2

Comparison of ^{31}P NMR Data of the Prepared Transition-Metal Complexes in Solution and in the Solid Silica Matrix

Complex	Solution ^{31}P NMR δ/ppm	^{31}P CP MAS NMR δ/ppm
$IrCl\{PPh_2(CH_2)_2Si(OEt)_3\}_3$	−13.0, −1.8[a]	−17.3, 4.9
$RhCl\{PPh_2(CH_2)_2Si(OEt)_3\}_3$	30.6, 46.9[b]	39.2
cis-$PtCl_2\{PPh_2(CH_2)_2Si(OEt)_3\}_2$	11.8[b]	10.3
cis-/*trans*-$PdCl_2\{PPh_2(CH_2)_2Si(OEt)_3\}_2$	*cis*: 32.3[b]	*cis*: 30.8
	trans: 22.0	*trans*: 21.3

[a] Solution spectrum in C_6D_6.
[b] Solution spectrum in $CDCl_3$.

that reported by Schubert *et al.* (27) with modified gelation conditions adjusted to the precursors used gave best results. The molar ratio metal complex: TEOS was varied from 1 : 20 to 1 : 50. High silica amounts were chosen for good fixation of the complexes within a stable matrix and to minimize negative interactions of neighboring complex molecules. Lower molecular ratios than 1 : 20 resulted in leaching of the catalyst, as indicated by colored washing liquids. The metal contents of the catalysts, calculated on the basis of metal used for preparations and amount of sample obtained after drying, varied from 1.7–9.2 wt%.

The resulting raw materials were glassy and clear, indicating a macroscopically homogeneous distribution of the complexes. The acids could be washed out completely after gelation. For the RuMe-catalysts no gelation procedure leading to clear gels could be found. Precipitation always occurred after addition of any kind of acid, base, or water. In contrast to the partly air sensitive complex precursors, all hybrid gel catalysts could be stored under ambient atmosphere after the sol-gel process.

Structural Properties of Hybrid Gels

NMR-spectroscopy. The ^{31}P NMR spectra of the complex precursors in solution were compared with CP/MAS measurements of the prepared catalysts to confirm the undestructed incorporation of the complexes (Table 2). The solid state NMR spectra were poorly resolved compared to the liquid NMR spectra. The half width at full intensity of the central component was about 15–20 ppm for the incorporated palladium complex and even broader for the other compounds. Note that differences in the position of the peaks are possibly due to the deviation of the liquid matrices from the solid silica matrices. Moreover, coalescence of peaks resolved in the solution spectra is observed for the solid spectra (Rh-complex).

Upon immobilization of the palladium complex the geometry about the metal center apparently changed from predominantly *trans* in the solution spectrum to predominantly *cis* in the solid state spectrum (Fig. 1). No conversion of the geometry about the metal center is reported in previous investigations (46). Based on these results no clear assignment can be made. The two most feasible explanations are the distortion of the true concentrations by the CP-technique rather than a real change in geometry, or alternatively, reversing the highfield/downfield shifts of the *cis* and *trans* structures in the solid matrix.

The structure of the silica network of catalysts RuMe-1 and RuMe-3 (Table 1) was investigated by ^{29}Si NMR measurements. In Fig. 2 the SPE-spectrum of catalyst RuMe-3 is shown as an example. Two groups of peaks are observed in the spectrum, corresponding to silicon species with four oxygen neighbors (Q-type species) and with three oxygen neighbors (T-type species), respectively. Q-type species originate from TEOS, whereas T-type species are derived from the silylether complex. After deconvolution of the peaks, silicon atoms with different degrees of condensation can be distinguished, corresponding to Si centers bridged via -O- linkages to one (T^1), two (Q^2, T^2), three (Q^3, T^3), and four (Q^4) nearest neighbors. Typical isomer

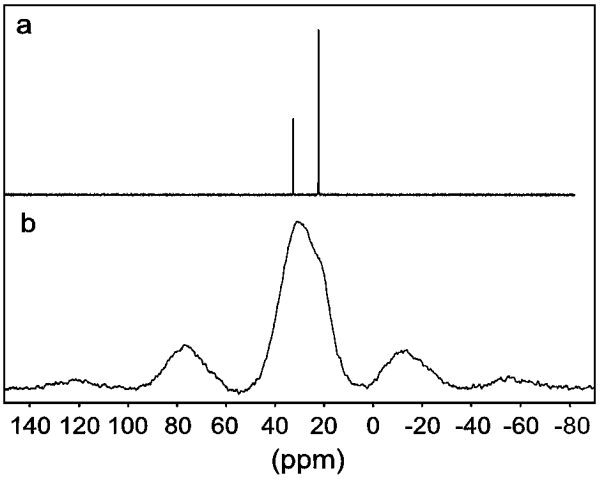

FIG. 1. Comparison of the ^{31}P NMR spectrum of $PdCl_2\{PPh_2(CH_2)_2Si(OEt)_3\}_2$ in solution (**a**) with the ^{31}P CP/MAS NMR spectrum of this complex co-condensed with tetraethoxysilane (**b**).

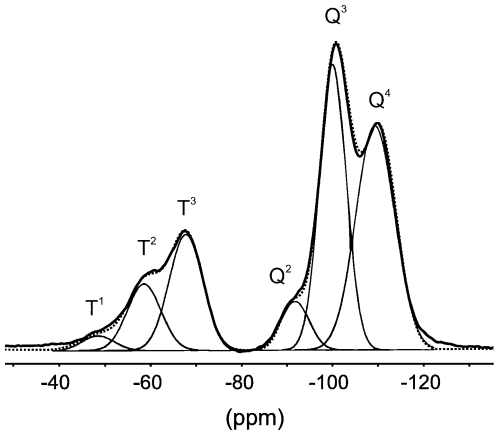

FIG. 2. ^{29}Si NMR spectrum (SPE) of a hybrid-gel catalyst (RuMe-3) prepared from $RuCl_2\{PMe_2(CH_2)_2Si(OEt)_3\}_3$. Peaks are divided into two groups, referring to silicon species derived from tetraethoxysilane (Q-species, right side) and from silylether ligands, belonging to ruthenium species (T-species, left side). Peaks are assigned to corresponding silicon species. Deconvoluted peaks used for integrating of the different silicon species are shown. The simulated spectrum (dotted line), which is the sum of the deconvoluted peaks, illustrates the good match of simulated and measured spectra.

shift values were −48.5/−58.5/−67.5 ppm for the $T^1/T^2/T^3$ signals, and −91.5/−101.5/−110 ppm for the $Q^2/Q^3/Q^4$ signals. For catalyst RuMe-3, prepared with acetic acid and a complex:TEOS ratio of 1 : 20, the respective fractions of the different structural units were 46% Q^4 $\{Si(OSi)_4\}$, 34% Q^3 $\{(HO)Si(OSi)_3\}$, 4.6% Q^2 $\{(HO)_2Si(OSi)_2\}$, 7.4% T^3 $\{RSi(OSi)_3\}$, 5.4% T^2 $\{R(HO)Si(OSi)_2\}$, and 2% T^1 $\{R(HO)_2SiOSi\}$. Catalyst RuMe-1, prepared with orthophosphoric acid and a complex, TEOS ratio of 1 : 50, consisted of 55% Q^4, 30% Q^3, 2.7% Q^2, 6.4% T^3, 4.8% T^2, and 1.8% T^1 species, indicating that a smaller part of the gel was uncondensed. The usage of a weaker acid with catalyst RuMe-3 decreased the ratio of completely condensed Q^4 species to Q^3 species from $Q^4/Q^3 = 1.83$ (catalyst RuMe-1) to $Q^4/Q^3 = 1.35$.

Further important information about the gel structure was obtained from ^{29}Si CP/MAS NMR measurements. Performing a cross-polarization (CP) experiment under Hartmann–Hahn conditions enabled much shorter measurement times in comparison to the ^{29}Si NMR investigations described above. With this technique, polarization of hydrogen is transferred to the silicons in a T_2-type process (spin–spin process), requiring only short contact times (T_C in the millisecond range). The CP transfer can be repeated quickly and, thus, allows fast data accumulation (33).

Various contact times T_C lead to different peak integrals in the spectra; thus, direct quantification of the different silicon species is not possible. The observed signal intensities $I(T_C)$ depend on the real amount of silyl species I_0, according to

$$I(T_C) = I_0/(1 - T_{SiH}/T_{1\varrho H})(e^{-T_C/T_{1\varrho H}} - e^{-T_C/T_{SiH}}). \quad [3]$$

The relaxation parameters T_{SiH} and $T_{1\rho H}$ determine dynamic properties of the silicon species, providing additional information about the local environment of the different silicon species. For the application of Eq. [3] these parameters have to be determined. The $T_{1\rho H}$ value describes the loss of proton magnetization in the rotating frame and, thus, depends on the mobility of the observed species on the NMR time scale. $T_{1\rho H}$ corresponds to the averaged relaxation of the protons within 1–2 nm, due to the exchange of spin energy within this range (48). Thus, different $T_{1\rho H}$ values indicate separate units of at least 1–2 nm size. Species with the same $T_{1\rho H}$ value should be bound to each other and should be homogeneously distributed.

The proton relaxation time in the rotating frame $T_{1\rho H}$ was measured via ^{29}Si with a separate experiment described by Schaefer *et al.* (33). Investigating catalyst RuMe-1, a monoexponential decay was found for the T^3 species, resulting in a constant $T_{1\rho H}$ value of 7.0 ms (Fig. 3). On the contrary, a multi-exponential decay could be observed for the Q^4 and Q^3 silicon species. The shape of the curve can be expressed by the sum of two or three exponential components, each characteristic of a different type of Q^4 and Q^3 type silicon species. Assuming three exponential components, three spatial regions of Q^4 species with $T_{1\rho H}$ relaxation times of 5.8, 8.8, and 13.3 ms, and three regions of Q^3 species with relaxation times of 4.9, 10.0, and 14.0 ms could be distinguished, thus, making the application of Eq. [3], requiring constant parameters, not reliable.

Extended X-ray absorption fine structure (EXAFS). To gain further information on the structure and state of the organometallic complexes after their immobilization in a silica matrix X-ray absorption spectroscopic measurements were carried out at the absorption edge of the respective transition metal. For determining the short-range order around the metal atom within the different hybrid gels the EXAFS was analyzed for at least one representative of each group (Fig. 4). Figure 5 illustrates the evaluation of the respective EXAFS spectra $\chi(k) \cdot k^3$ of the iridium

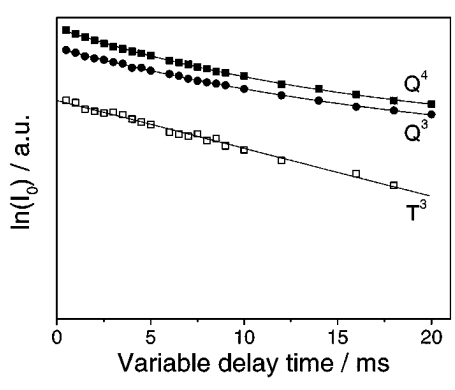

FIG. 3. Determination of $T_{1\rho H}$ parameter for a hybrid-gel catalyst (RuMe-1) prepared from $RuCl_2\{PMe_2(CH_2)_2Si(OEt)_3\}_3$.

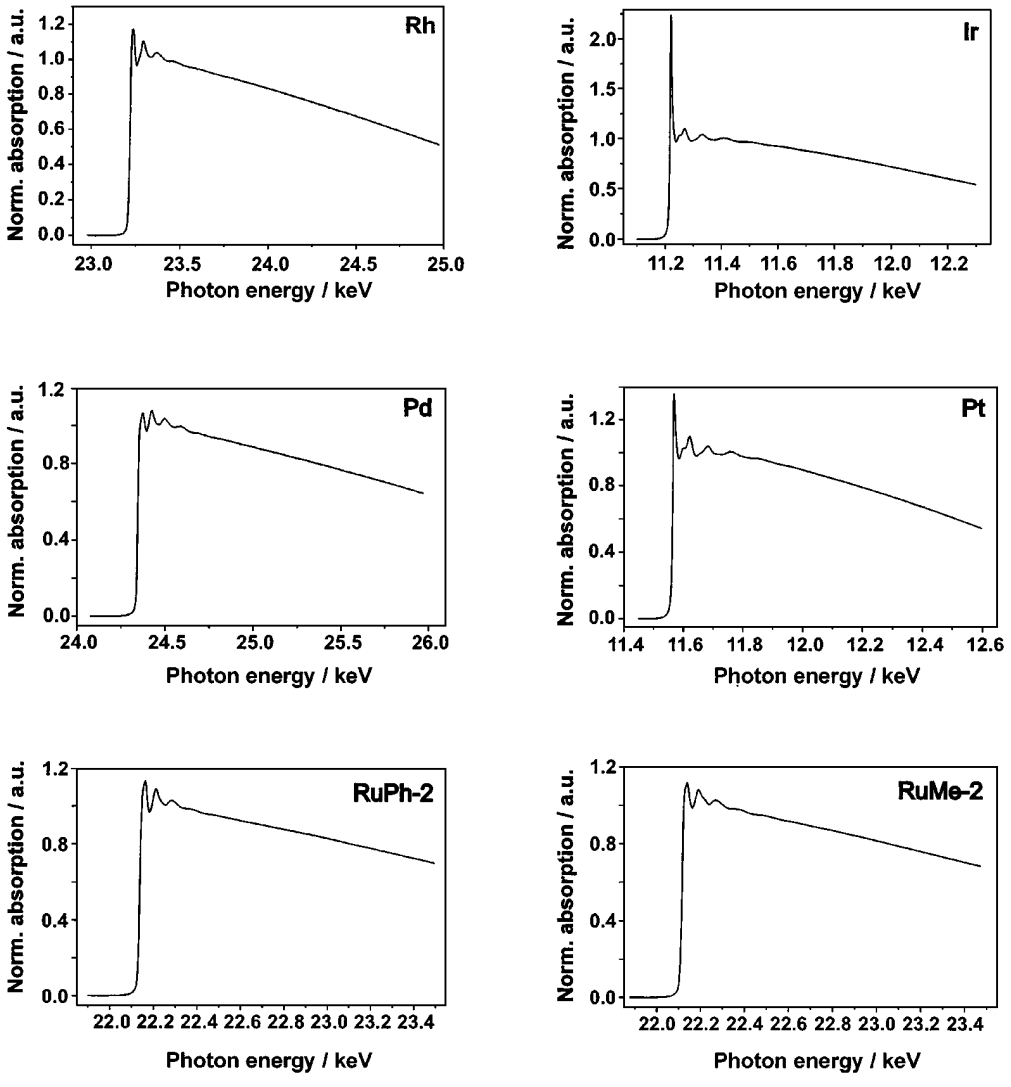

FIG. 4. Extended X-ray absorption fine structures of representative hybrid-gel catalysts. (For other properties cf. Table 1).

containing catalyst (Ir) by Fourier transformation (modified radial distribution functions) and fitting with theoretical amplitude and phase functions. The Fourier transforms of the EXAFS spectra of the catalysts RuPh-2, prepared from $RuCl_2\{PPh_2(CH_2)_2Si(OEt)_3\}_3$, and RuMe-2, prepared from $RuCl_2$-$\{PMe_2(CH_2)_2Si(OEt)_3\}_3$, are depicted in Fig. 6. All hybrid gels show in general only one coordination shell except for Pt, which exhibits a small additional peak at approximately 4 Å caused by weak Pt–Pt interactions or multiple scattering effects within the shell of next-nearest neighbors. For all other catalysts no metal–metal interaction was found, thus excluding dimerization or oligomerization reactions during the sol-gel process.

In one of the fits reasonable structural parameters could be obtained by fitting the first shell with just one type of ligand (P or Cl or O). Best results were achieved by refining a M-P and a M-Cl shell simultaneously in a two-shell fit (see Table 3). The number of metal–phosphine interactions in hybrid gel catalysts containing Rh, Ir, Pd, and Pt are the same as in the precursor complexes, giving additional evidence for their undestructed immobilization. For the RuPh catalysts (ruthenium with phenyl phosphine ligands) the predicted coordination numbers are also found within the accuracy of the method, confirming the proposed structure of the ruthenium complexes in solution and in the solid matrix. Note that for these samples tendentiously negative deviations from the theoretical coordination number are found. In contrast to the catalysts containing phenyl phosphine ligands the calculated coordination number for catalyst RuMe-2, made from $RuCl_2\{PMe_2(CH_2)_2Si(OEt)_3\}_3$, was 1 less than in the proposed precursor structure, indicating that only two phosphine ligands are bonded to each ruthenium center.

Transmission electron microscopy (TEM). For a more detailed morphological and structural characterization, the

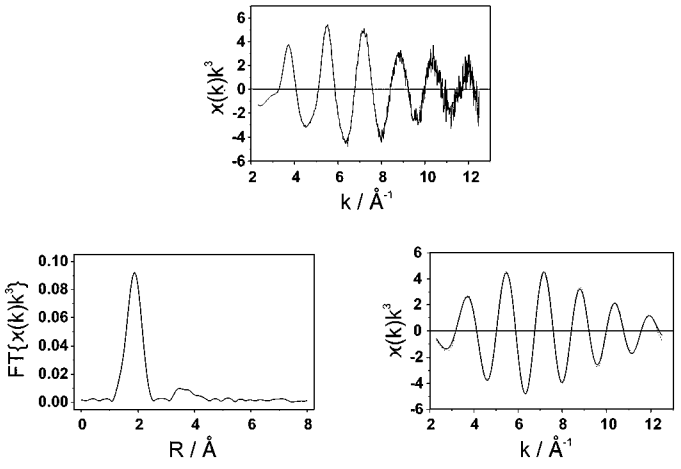

FIG. 5. The evaluation of the EXAFS information is shown in the example for the iridium-containing catalyst (Ir). The extracted edge information (top) is Fourier transformed (bottom left), after which the first shell is back-transformed (bottom right, straight line) and fitted with theoretical amplitude and phase functions (dotted line).

catalysts RuPh-1, RuPh-2, RuMe-2, and RuMe-3 were investigated by TEM. All samples were completely amorphous, as evidenced by the representative TEM image of sample RuPh-2 shown in Fig. 7. Neither crystalline moieties of silica nor any indication for the presence of ruthenium particles were seen, corroborating that ruthenium was finely distributed within the silica matrix. Moreover, electron diffraction yielded no distinct reflections, proving the noncrystallinity of the catalyst.

X-ray diffraction (XRD). Figure 8 shows the X-ray diffraction patterns of the samples Rh, Ir, Pd, Pt, RuPh-2, RuMe-1, and RuMe-3. All diffractograms were similar, exhibiting only broad bands but no sharp reflections, corroborating the amorphicity of the materials.

Nitrogen and argon physisorption. Nitrogen physisorption experiments were carried out to investigate the influence of the structure and the concentration of the incorporated complexes on the surface area and the pore size distribution of the final hybrid gels. According to IUPAC classification (49), the catalysts showed, in general, a type-IV physisorption isotherm with a more or less pronounced type-I isotherm character, indicating mesoporous solids with a strong contribution of microporosity. Corresponding t-plot constructions confirmed the presence or absence

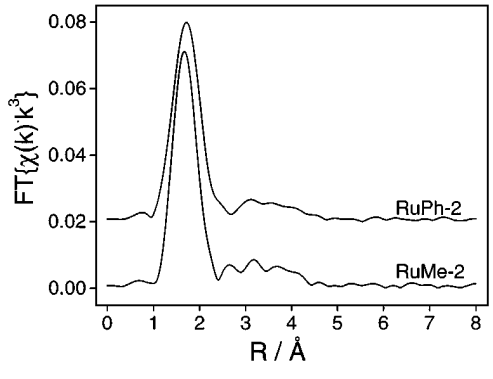

FIG. 6. Fourier transforms of the EXAFS of ruthenium containing catalysts with phenylphosphine (RuPh-2) and methylphosphine (RuMe-2) ligands, respectively.

TABLE 3

Refined Structure Parameters for the Metal-Phosphorus (M-P) and Metal-Chlorine (M-Cl) Bonds within the First Coordination Shell of the Immobilized Metal Complexes

	M-P			M-Cl		
Catalyst	N	R/Å	$\Delta\sigma^2$/Å^2	N	R/Å	$\Delta\sigma^2$/Å^2
RuPh-1	2.83	2.269	0.0052	1.88	2.382	0.0042
RuPh-2	2.75	2.273	0.0047	1.89	2.389	0.0037
RuMe-2	2.06	2.191	−.0035	1.72	2.299	−0.0037
Ir	2.96	2.267	0.0047	0.95	2.348	0.0012
Rh	2.75	2.225	0.0021	1.15	2.346	−0.0005
Pt	2.02	2.227	0.0020	1.92	2.330	0.002
Pd	1.95	2.245	−0.0022	1.94	2.356	−0.0021

Note. N = coordination number, R = bond length, $\Delta\sigma^2$ = Debye–Waller factor.

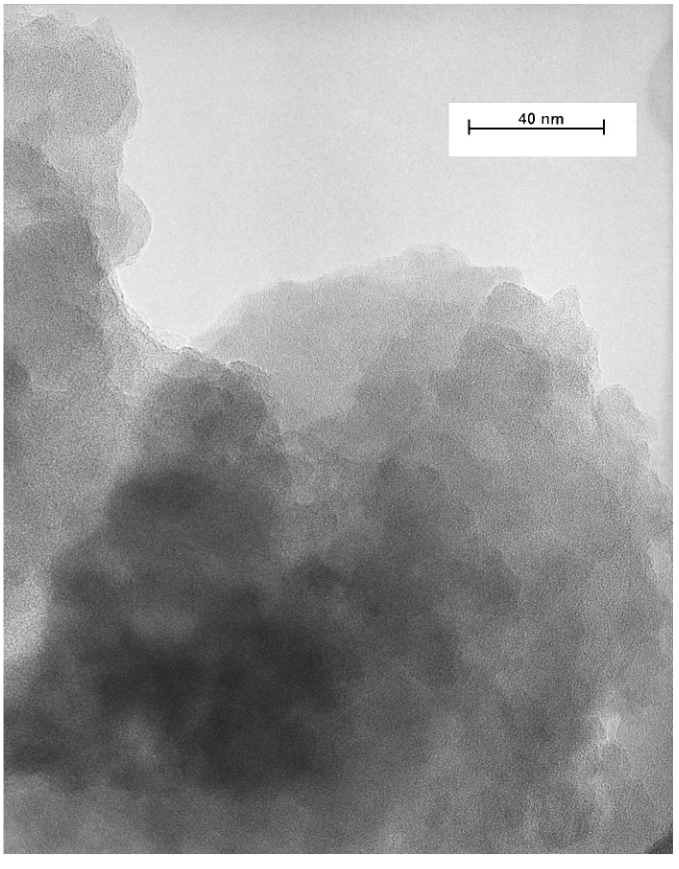

FIG. 7. Transmission electron micrograph of a hybrid-gel catalyst prepared from $RuCl_2\{PPh_2(CH_2)_2Si(OEt)_3\}_3$.

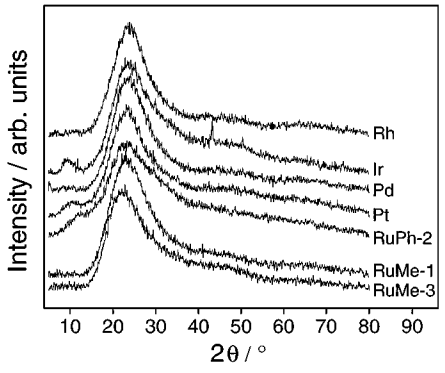

FIG. 8. X-ray diffraction patterns of hybrid-gel catalysts containing different group(VIII metals.

of microporosity. No desorption hysteresis (pure type-I isotherm) and, therefore, predominantly microporous character of the solids was observed for catalysts Ir and Pd. Sample Pt revealed pronounced type-H2 desorption hysteresis, whereas for the other samples only weak type-H2 or -H4 desorption hysteresis was observed, indicating different degrees of mesoporosity. From the data listed in Table 1 it can be seen that S_{BET} was highest for pure silica (880 $m^2 \cdot g^{-1}$). The surface area of the catalysts prepared with a complex : TEOS ratio of 1 : 50 varied within a range of 430 to 800 $m^2 \cdot g^{-1}$. For the ruthenium catalysts the structure of the immobilized complex and the amount of complex used had a pronounced influence on the surface area. Higher metal loadings resulted in significantly lower surface areas. Note that catalysts made from $RuCl_2\{PMe_2(CH_2)_2Si(OEt)_3\}_3$ with a complex : TEOS ratio of 1 : 20 afforded markedly different BET surface areas, because precipitation occurred during the preparation of gels. When the preparations were repeated, S_{BET} could be reproduced within ±5%. The contribution of the micropore surface area, determined by argon physisorption, is also listed in Table 1 for selected samples.

Typical pore size distributions of the catalysts are shown in Fig. 9. Pure silica and the platinum-containing catalyst exhibited only mesoporosity with distinct maxima between

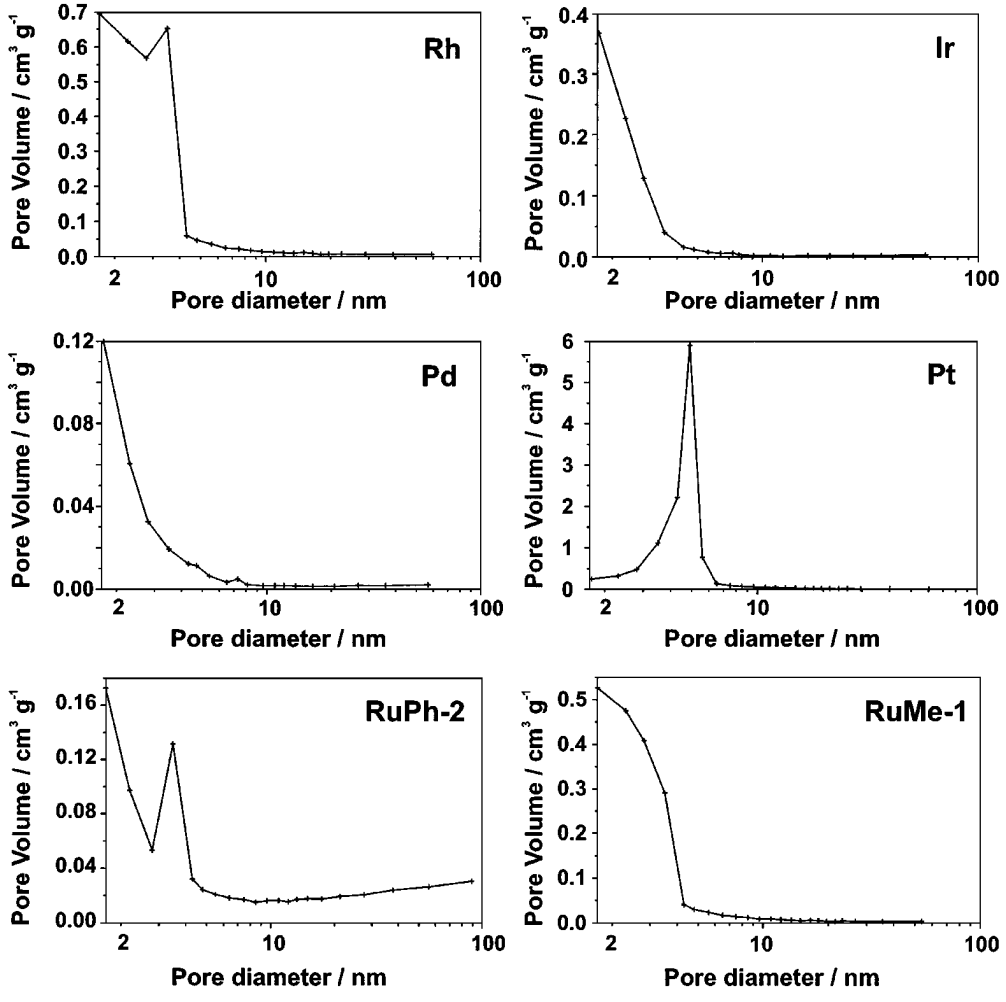

FIG. 9. Textural properties of sol-gel immobilized group(VIII) transition metal complexes. Differential BJH pore size distributions {dV/dlog(D)} derived from the desorption branches of the physisorption isotherms.

3.5 and 4.8 nm. Similar maxima could also be found for the samples Rh, RuPh-2, and RuMe-3, but in these cases with a significant contribution of micropores. The other materials exhibited transition from micro- to mesoporosity, discernible from the constantly sloping curve of the BJH-plot (e.g. catalysts Ir, Pd, and RuMe-1). Catalyst RuPh-2 showed an exceptional BJH-plot with a slightly rising curve for larger pores. Thus, a combination of micro-, meso-, and macropores is found for this catalyst. Corresponding mean pore diameters of the catalysts are listed in Table 1.

Catalytic Properties of Hybrid Gels

The hybrid gel catalysts were tested for the solvent-free synthesis of *N,N*-dimethylformamide and methyl formate, respectively, from carbon dioxide. Under the experimental conditions applied, the CO_2/H_2 mixture was in the supercritical region, whereas due to their low solubility in $scCO_2$ (50, 51), dma (methanol/triethylamine), and the products dmf (mf) and water were in the liquid state (17). High swelling of the liquid dma phase by dissolved CO_2 was reported by Jessop *et al.* (17), thus providing high local concentrations of reactants at the surface of the catalysts, which are in the liquid phase at the bottom of the reactor.

Synthesis of N,N-dimethylformamide. All catalysts were found to be stable under reaction conditions, except Rh and Ir, whose color changed during reaction. GC analysis of the liquid phase indicated the production of dmf with 100% selectivity in all cases, except for Pt, which produced trace amounts of trimethylamine as a by-product. Trimethylamine can be formed as a thermodynamically favored disproportionation product from the dimethylamine reactant or by overreduction of dmf. No by-products could be detected in the gas phase, showing that neither CO formation by the reverse water–gas shift reaction nor methane synthesis occurred under the conditions used. At low conversions a white precipitate was obtained after pressure release, which melted within approximately one hour under degassing. GC analysis of this product showed signals characteristic for dimethylamine and CO_2, respectively, indicative of a carbamate compound.

Results of the catalytic tests are summarized in Table 4. The data provide a qualitative ranking of the catalytic behavior of the different hybrid gels. Pure silica (Si) was tested as a reference and exhibited no catalytic activity. Comparing the different transition metal catalysts reveals that the activity, expressed as turnover frequency (TOF), decreases in the order Ru > Ir > Pt,Pd > Rh. The rhodium catalyst (Rh) exhibited only low activity and decomposed under reaction conditions by producing black metallic deposits on the wall of the autoclave. Although the iridium catalyst (Ir) changed its color from beige to white during reaction, indicating structural alteration, its activity remained high.

Regarding the influence of the silylether ligand of the ruthenium complex, the use of methylphosphine ligands (RuMe) resulted in more active catalysts, as compared to phenylphosphine ligands (RuPh), independently of the preparation conditions. However, a different effect of metal

TABLE 4

Catalytic Properties of Sol-Gel Derived Hybrid Gels in the Synthesis of *N,N*-Dimethylformamide (dmf) from Carbon Dioxide, Hydrogen, and Dimethylamine

				dmf			
Catalyst	Complex	Complex : TEOS	Acid	TON[a]	TOF/h^{-1}[b]	Yield/%	Selectivity/%
Si	—	0 : 100	H_3PO_4	0	0	0	0
RuPh-1	$RuCl_2\{PPh_2(CH_2)_2Si(OEt)_3\}_3$	1 : 50	H_3PO_4	3230	220	25	100
RuPh-2	$RuCl_2\{PPh_2(CH_2)_2Si(OEt)_3\}_3$	1 : 20	H_3PO_4	4420	290	35	100
RuMe-1	$RuCl_2\{PMe_2(CH_2)_2Si(OEt)_3\}_3$	1 : 50	H_3PO_4	13670	900	94	100
RuMe-1[c]	$RuCl_2\{PMe_2(CH_2)_2Si(OEt)_3\}_3$	1 : 50	H_3PO_4	110800	1860	82	100
RuMe-2	$RuCl_2\{PMe_2(CH_2)_2Si(OEt)_3\}_3$	1 : 20	H_3PO_4	11800	790	84	100
RuMe-3	$RuCl_2\{PMe_2(CH_2)_2Si(OEt)_3\}_3$	1 : 20	$MeCO_2H$	11870	800	92	100
Ir	$IrCl\{PPh_2(CH_2)_2Si(OEt)_3\}_3$	1 : 50	$MeCO_2H$[e]	2900	190	23	100
Rh	$RhCl\{PPh_2(CH_2)_2Si(OEt)_3\}_3$	1 : 50	$MeCO_2H$[e]	530	35	4	100
Pt	$PtCl_2\{PPh_2(CH_2)_2Si(OEt)_3\}_2$	1 : 50	H_3PO_4	1490	100	10	98[d]
Pd	$PdCl_2\{PPh_2(CH_2)_2Si(OEt)_3\}_2$	1 : 50	$MeCO_2H$	1410	90	11	100

Note. Reaction conditions: 500-ml stainless-steel autoclave; $n[Me_2NH] = 0.71$ mol; $p[H_2] = 8.5$ MPa; $p[CO_2] = 13.0$ MPa; $T = 373$ K; $t = 15$ h; stirring rate = 300 min^{-1}; n[catalyst] = 5×10^{-5} mol (expressed as amount of group(VIII) metal).

[a] TON = mol dmf · (mol complex)$^{-1}$.

[b] TOF = TON · h^{-1}.

[c] $n[Me_2NH] = 6.4$ mol , $T = 406$ K, $t = 60$ h, stirring rate = 500 min^{-1}, n[catalyst] = $1.8 \cdot 10^{-5}$ mol. Due to the pressure drop in the reactor, H_2 and CO_2 had to be recharged regularely.

[d] By-product trimethylamine.

[e] Change of active species under reaction conditions.

loading on activity was observed for the two ligands. Whereas the turnover frequency of the ruthenium catalyst with phenylphosphine ligands increased with higher metal loading, the opposite behavior was found for the methylphosphine ligand. The use of either phosphoric acid or acetic acid in the sol-gel process had no significant effect on the catalytic performance of the ruthenium-containing hybrid gels. With a ruthenium catalyst containing methylphosphine ligands (RuMe-1), a maximum turnover number (TON) of 110,800 at 100% selectivity was attained under specific conditions (Table 4).

The color of the ruthenium catalysts after catalytic testing was significantly brighter than prior to testing. Leaching of active species from the catalysts could be neglected, since the liquid product exhibited no catalytic activity in a subsequent activity test. Moreover, using the same ruthenium catalyst for three consecutive experiments resulted in a marked increase of catalytic activity for the second run, which remained stable in the third experiment. This behavior can presumably be attributed to the formation of an active hydrido intermediate formed by hydrogenolysis of the ruthenium-chlorine bond under reaction conditions. The good stabilizing effect of the sol-gel process on homogeneous complexes was supported by the long lasting activity of the tested complexes. Fresh, as well as used, catalysts containing hydrido species, which were used for catalytic testing after storage under air for one year, showed no loss of activity. This contrasts the findings with homogeneous analogues, where the reaction mixtures rapidly changed their color or precipitates formed, indicating decomposition of the complexes.

Synthesis of methyl formate. Catalyst RuMe-1, the most active catalyst in dmf production, was also tested in the synthesis of methyl formate (Table 5). In a series of nonoptimized experiments methyl formate was produced very efficiently at a selectivity of 100%. A maximum TOF of 115 h^{-1} was reached, which is more than two times better than the best reported homogeneous result (17). When increasing the reaction time to 64 h, the TON was higher but the TOF decreased to about 50 h^{-1}. The maximum in activity was found at 373 K. For lower and higher temperatures the rate of the reaction decreased, which is in good agreement with the observation of Jessop *et al.* (17), who found an optimum temperature of 353 K for the homogeneously catalyzed reaction.

The utilization of an additional base (triethylamine) was crucial to reach high yields of methyl formate. Without base methanol conversions were low. However, a molar ratio of methanol : base of 10 : 1 was enough to reach high activities in methyl formate synthesis. Addition of γ-alumina as an acidic catalyst for the esterification, instead of base led only to low yields of methyl formate.

DISCUSSION

Structural Properties of Hybrid Gel Catalysts

For the immobilization of sensitive transition metal complexes mild gelation conditions are required to prevent destruction of the complexes. A modified method of Schubert *et al.* (27), utilizing mild acidic conditions at room temperature was found to be most suitable for our complexes. Ageing at the end of the sol-gel process was necessary to obtain stable gels, which do not undergo leaching upon washing with water or acetone. During ageing the degree of condensation of the network increases by polycondensation of part of the remaining free hydroxyl groups.

The immobilization of the metal complexes was followed using ^{31}P NMR spectroscopy. Because of the anisotropy, which cannot be averaged out in the solid phase, solid state spectra were always less resolved than the corresponding liquid spectra. Moreover, the characteristic peaks were always broader than the expected intrinsic minimum peak width of solid state spectra. This shift dispersion originates, if the environments for the immobilized complexes are quite different and disordered, as anticipated from the gelation procedure. For the platinum-containing catalyst the

TABLE 5

Catalytic Properties of the Hybrid-Gel RuMe-1 Derived from $RuCl_2\{PMe_2(CH_2)_2Si(OEt)_3\}_3$ in the Synthesis of Methyl Formate from Carbon Dioxide, Hydrogen, and Methanol

n[Catalyst]/μmol[a]	n[Methanol]/mol	n[Triethylamine]/mol	t/h	T/K	TON[b]	TOF/h^{-1}[c]
17.2	0.74	0.074	15	353	790	53
14.1	0.74	0.074	15	393	1270	85
17.7	0.75	0.074	15	373	1740	115
17.6	0.99	0.074	64	373	3180	50
17.3	0.74	$1.0 \cdot 10^{-3}$[d]	15	373	75	5

Note. Reaction conditions: 500-ml stainless-steel autoclave; $p[H_2] = 8.5$ MPa; $p[CO_2] = 13.0$ MPa; stirring rate = 300 min^{-1}.

[a] n[catalyst] expressed as amount of ruthenium complex.

[b] TON = mol methyl formate · (mol complex)$^{-1}$.

[c] TOF = TON · h^{-1}.

[d] Additive = γ-Al_2O_3.

peaks were narrower than in the other cases, indicating a more uniform incorporation of the complexes.

The transparency of the obtained glass-like colored solids indicated a macroscopically homogeneous distribution of the complexes in the silica matrix. TEM investigations of the finely powdered gels corroborated the complete homogeneity and the amorphous structure of the materials. EXAFS measurements proved the unchanged immobilization of the nonruthenium precursors. For the ruthenium catalysts containing phenyl phosphine ligands (RuPh), the proposed penta-coordinated structure of the ligand sphere was also confirmed. The small negative deviations from the theoretical coordination numbers in these catalysts can be attributed to minor ligand cleavage in solution during the sol-gel process. James and Markham observed for a similar complex that, in a 1 *N* solution of $RuCl_2(PPh_3)_3$ in benzene, 80% of the complex is dissociated (47, 52). The substantial deviation of 1 in the coordination sphere for catalyst RuMe-2 from the proposed precursor structure $RuCl_2\{PMe_2(CH_2)_2Si(OEt)_3\}_3$ revealed that only two phosphine ligands are bound to each ruthenium center, indicating the dissociation of a phosphine ligand during immobilization (47). Based on EXAFS measurements, all complexes in the hybrid gels are monomers. Dimerization and oligomerization reactions of the precursors during the sol-gel process can be excluded, since no metal–metal interactions are found (except for Pt). In contrast to the heterogenization of silylether metal complexes by the sol-gel method used which results in a homogeneous distribution of the metal moieties throughout the material, clustering of the metal is observed for the classical sol-gel route. Lopez *et al.* used $RuCl_3$ in a sol-gel process for the production of highly dispersed ruthenium in silica (53). The corresponding TEM micrographs showed small particles of ruthenium within a silica support.

The highly disordered structure of the gels was corroborated by ^{29}Si SPE NMR measurements. The direct detection of the ^{29}Si nuclei enabled the reliable quantification of the different silicon species by integration of the deconvoluted peaks. The accuracy of this method is estimated to be about $\pm 5\%$ (29). However, the slow relaxation of the ^{29}Si nuclei resulted in long repetition times of about 200 s, making SPE measurements very time consuming.

The alternative quantification of the different silicon species by CP measurements was difficult due to the great part of silica in the catalyst. In this silica, moieties of condensed Q^4 species, silicon atoms which are more than four single bonds distant from the next proton, make nearly no contribution to the peak intensity, due to the low cross-polarization efficiency (29). Deviations of more than 20% were obtained for the Q^4 species, when results of CP/MAS measurements and SPE experiments were compared. In the case of high amounts of silica without contribution to signal intensity and species with different mobility, SPE experiments should be preferred for a reliable quantification of different species.

A rough picture of the gel structure can be drawn from the NMR data available. The gels consist of ruthenium species and silicon species, which are incompletely condensed. The great part of incompletely condensed silicon species (Q^3, Q^2, T^2, T^1) indicates a highly disordered structure. Large amounts of Q^4 species, not detectable by CP/MAS measurements, indicate areas of bulk-Q^4-species, more than four single bonds distant from the next proton. All ruthenium species are equally bound to their environment due to the constant $T_{1\rho H}$ value for the T^3 species, indicating a homogeneous distribution of ruthenium and silicon species. On the contrary, the ruthenium species are surrounded by at least three different Q^4 and Q^3 species, with $T_{1\rho H}$ values lower, higher, and in the same range than for the T^3 species. Higher $T_{1\rho H}$ values indicate spatial regions of bulk-Q^4-species, related to pure amorphous silica. This observation is in good agreement with the high amount of invisible silica, more than four bonds distant from next proton.

Regarding the surface area and porosity of the different hybrid gels, the data listed in Table 1 and shown in Fig. 9 for similarly prepared samples varied over a wide range, indicating a pronounced influence of the structures of the immobilized group(VIII) metal complexes on the textural properties of the gels. Possible reasons are the different size and geometry of the complexes and, thus, a disturbance of the network structure in different ways. A correlation between the average pore diameter, which varied in the range 1.9–5.3 nm, and the preparation conditions is not discernible in general. For the Ru containing gels lower surface areas are found for higher complex loadings. This observation is in agreement with findings of Schubert *et al.* (27), who investigated the interrelation between complex concentration and specific surface area for a cobalt complex immobilized by a similar method. Possible explanations for this behavior are (i) easier relaxation of the polymeric network by the introduction of the complexes, (ii) the influence of the steric demand of the complexes on particle growth, or (iii) electronic influences of the alkyl chain in the silylether ligand on its reactivity in the sol-gel process (27). The small surface areas, found for RuMe-2 and RuMe-3, are due to precipitation, which occurred when the acid was added for gelation, rendering control of the gelation conditions difficult.

Catalytic Properties of Hybrid Gel Catalysts

Synthesis of N,N-dimethylformamide. Among all sol-gel derived hybrid materials, ruthenium-containing silica gels showed highest activity in dmf synthesis from CO_2, H_2, and dma. No correlation between surface area and catalytic activity of the catalysts could be observed. Catalysts RuMe-2 with a surface area of $<5\ m^2 \cdot g^{-1}$ and RuMe-3

with 70 $m^2 \cdot g^{-1}$ exhibited comparable catalytic activity to catalyst RuMe-1 with 510 $m^2 \cdot g^{-1}$.

The white solids or highly viscous liquids obtained after catalytic tests at low conversions in dmf synthesis can be best described as Dimcarb (54), an addition compound of CO_2 with dimethylamine of variable stoichiometry. Dimethylammonium *N,N*-dimethylcarbamate, the precise 2 : 1 complex, has a melting range between 30 and 45°C.

The elucidation of the phase behavior inside the reactor is of crucial importance to explain the high efficiency of the described reaction design. Under similar reaction conditions Jessop *et al.* (17) observed high swelling of the liquid phase, if a supercritical phase is present. Leitner also stated that high pressures are required for swelling of the liquid phase, but the gases do not have to be in the supercritical state for reaching this behavior (55). This means for our system that high local concentration of dma, CO_2, and H_2 are provided at the catalyst surface. On the contrary, only small amounts of amine were found in the gas phase (17), indicating that the liquid phase can favorably be used as the reaction phase. In a study with homogeneous ruthenium complexes we could confirm the high efficiency of this reaction design also at subcritical conditions (19).

Upon catalytic testing the color of the catalysts became brighter, probably indicating the formation of colorless hydrido complexes. This assumption is supported by the even higher activity of the catalysts in a second and third run. Hydrido complexes are known to be active catalysts in homogeneous hydrogenations (32). They are simply formed from ruthenium dichloro phosphine complexes by hydrogenation in the presence of organic bases (32, 56). For similar ruthenium chloro phosphine complexes used in the homogeneous synthesis of dmf and methyl formate the monohydrido complex could be identified as an intermediate (17, 19, 57).

Synthesis of methyl formate. Investigation of the methyl formate synthesis at different temperatures revealed a maximum TOF at 393 K. The formation of formic acid in a first reaction step is reversible, resulting in increasing decomposition to the reactants hydrogen and carbon dioxide at higher temperatures. In contrast, the subsequent esterification requires higher temperatures to proceed efficiently. This antagonistic effect results in the observed optimum temperature, enabling a sufficiently effective esterification of formic acid to methyl formate at relatively slow decomposition rates. The hybrid catalysts seem to meet these requirements, since the optimum temperature is shifted to higher values.

The addition of triethylamine as base is crucial for this reaction to obtain substantial amounts of methyl formate. 10 mol% of base promoted the reaction sufficiently. The base acts as a thermodynamic sink in the first step of the reaction, which stabilizes the intermediate formic acid under the severe conditions inside the reactor (58, 59). Only small amounts of methyl formate were found after addition of γ-alumina as an acidic esterification catalyst, suggesting a more pronounced effect of the stabilization of the formic acid after the first reaction step than the acceleration of the subsequent esterification (17).

The high reaction rates in methyl formate synthesis can again be explained by the favorable liquid phase reaction design. Comparable to the swelling of amines, the volume of the methanol phase increases at elevated pressures (17), resulting in high concentrations of hydrogen in the liquid methanol/triethylamine phase at the catalysts surface.

CONCLUSIONS

Sol-gel derived hybrid materials have been used as heterogeneous catalysts for the solvent-free synthesis of *N,N*-dimethylformamide and methyl formate utilizing supercritical CO_2 as both solvent and reactant. Highly active and stable catalysts were prepared by incorporation of specially tailored complexes of Ru, Rh, Ir, Pd, and Pt with bifunctional silylether phosphine ligands within a porous silica network applying the sol-gel method.

The ruthenium-containing hybrid gel catalysts proved to be 100% selective and most active for dmf synthesis, affording turnover numbers up to 110,800 with corresponding TOFs of 1860 h^{-1}. This turnover frequency exceeds those previously achieved with heterogeneous catalysts more than 600 times. The ruthenium catalysts also selectively catalyze the synthesis of methyl formate.

Textural investigations indicated that all hybrid gels were micro- to mesoporous, except the platinum-containing catalyst, which was predominantly mesoporous. TEM and XRD analysis proved the homogeneity and noncrystallinity of the materials. Valuable information concerning the bulk properties were obtained by solid state ^{29}Si NMR spectroscopy, revealing significant parts of incompletely condensed silicon species, indicative for a highly disordered structure of the gels. EXAFS investigations indicated that the transition metal complexes were immobilized as isolated entities. Nondestructive incorporation of the silylether complexes was corroborated by ^{31}P NMR and EXAFS.

ACKNOWLEDGMENT

Financial support of this work by the Bundesamt für Energiewirtschaft (Project 21180) is gratefully acknowledged.

REFERENCES

1. Behr, A., *in* "Catalysis in C_1 Chemistry" (W. Keim, Ed.), p. 169. D. Reidel, Dordrecht, 1983.
2. Behr, A., *Angew. Chem., Int. Ed. Engl.* **27**, 661 (1988).
3. Chinchen, G. C., Denny, P. J., Jennings, J. R., Spencer, M. S., and Waugh, K. C., *Appl. Catal.* **36**, 1 (1988).

4. Halmann, M., "Chemical Fixation of Carbon Dioxide: Methods for Recycling CO_2 into Useful Products," CRC Press, Boca Raton, FL, 1993.
5. Baiker, A., and Koeppel, R. A., *in* "Proceedings, International Conference on Carbon Dioxide Utilization, Bari, Italy, 1993," p. 295.
6. Jessop, P. G., Ikariya, T., and Noyori, R., *Chem. Rev.* **95**, 259 (1995).
7. Leitner, W., *Angew. Chem., Int. Ed. Engl.* **34**, 2207 (1995).
8. Haynes, P., Slaugh, L. H., and Kohnle, J. F., *Tetrahedron Lett.*, 365 (1970).
9. Inoue, Y., Sasaki, Y., and Hashimoto, H., *J. Chem. Soc., Chem. Comm.*, 718 (1975).
10. Kiso, Y., and Saeki, K., Japan, Kokai 77 36,617, 1977.
11. Kudo, K., Phala, H., Sugita, N., and Takezaki, Y., *Chem. Lett.*, 1495 (1977).
12. Phala, H., Kudo, K., Mori, S., and Sugita, N., *Bull. Inst. Res., Kyoto Univ.* **59**, 88 (1981).
13. Phala, H., Kudo, K., Mori, S., and Sugita, N., *Bull. Inst. Res., Kyoto Univ.* **63**, 63 (1985).
14. Schreiner, S., Yu, J. Y., and Vaska, L., *Inorg. Chim. Acta* **147**, 139 (1988).
15. Jessop, P. G., Ikariya, T., and Noyori, R., *J. Am. Chem. Soc.* **116**, 8851 (1994).
16. Jessop, P. G., Hsiao, Y., Ikariya, T., and Noyori, R., *J. Chem. Soc., Chem. Commun.*, 707 (1995).
17. Jessop, P. G., Hsiao, Y., Ikariya, T., and Noyori, R., *J. Am. Chem. Soc.* **118**, 344 (1996).
18. Kröcher, O., Köppel, R. A., and Baiker, A., *J. Chem. Soc., Chem. Commun.*, 1497 (1996).
19. Kröcher, O., Köppel, R. A., and Baiker, A., *J. Chem. Soc., Chem. Commun.*, 453 (1997).
20. Kröcher, O., Köppel, R. A., and Baiker, A., *Chimia* **51**, 48 (1997).
21. Jessop, P. G., Ikariya, T., and Noyori, R., *Nature* **368**, 231 (1994).
22. Kröcher, O., Köppel, R. A., and Baiker, A., *in* "Process Technology Proceedings" (Ph. Rudolf von Rohr and Ch. Trepp, Eds.), Vol. 12, p. 91. Elsevier, Amsterdam, 1996.
23. Murrell, L. L., *in* "Advanced Materials in Catalysis" (J. J. Burton and R. L. Garten, Eds.), p. 235. Academic Press, New York, 1977.
24. Whitehurst, D. D., *Chemtech.*, 44 (1980).
25. Deschler, U., Kleinschmitt, P., and Panster, P., *Angew. Chem.* **98**, 237 (1986).
26. Schubert, U., *New J. Chem.* **18**, 1049 (1994).
27. Schubert, U., Rose, K., and Schmidt, H., *J. Non-Cryst. Solids* **105**, 165 (1988).
28. Lindner, E., Bader, A., and Mayer, H. A., *Z. Anorg. Allg. Chem.* **598**, 235 (1991).
29. Lindner, E., Kemmler, M., Mayer, H. A., and Wegner, P., *J. Am. Chem. Soc.* **116**, 348 (1994).
30. Parshall, G. W., *Inorg. Synth.* **11**, 157 (1968).
31. Niebergall, H., *Makromol. Chem.* **52**, 218 (1962).
32. Harmon, R. E., Gupta, S. K., and Brown, D. J., *Chem. Rev.* **73**, 21 (1973).
33. Schaefer, J., Stejskal, E. O., and Buchdahl, R., *Macromolecules* **10**, 384 (1977).
34. Barrett, E. P., Joyner, L. G., and Halenda, P. P., *J. Am. Chem. Soc.* **73**, 37 (1951).
35. Broekoff, J. C. P., *Stud. Surf. Sci. Catal.* **3**, 663 (1979).
36. Lippens, B. C., and DeBoer, J. H., *J. Catal.* **4**, 319 (1965).
37. Dubinin, M., and Astakhov, V., *Adv. Chem. Ser.* **102**, 69 (1971).
38. Frahm, R., *Nucl. Instrum. Meth. Phys. Res. A* **270**, 578 (1988).
39. Ressler, T., *J. de Physique IV C* **2**, 269 (1997).
40. Rehr, J. J., Mustre de Leon, J., Zabinski, S. I., and Albers, R. C., *J. Am. Chem. Soc.* **113**, 5135 (1991).
41. Kröcher, O., Köppel, R. A., and Baiker, A., *J. Mol. Catal.*, in press.
42. Bemi, L., Clark, H. C., Davies, J. A., Fyfe, C. A., and Wasylishen, R. E., *J. Am. Chem. Soc.* **104**, 438 (1982).
43. Pregosin, P. S., and Kunz, R. W., "^{31}P and ^{13}C NMR of Transition Metal Phosphine Complexes." Springer-Verlag, Berlin, 1979.
44. Grim, S. O., Keiter, R. L., and McFarlane, W., *Inorg. Chem.* **6**, 1133 (1967).
45. Grim, S. O., and Keiter, R. L., *Inorg. Chim. Acta* **4**, 56 (1970).
46. Komoroski, R. A., Magistro, A. J., and Nicholas, P. P., *Inorg. Chem.* **25**, 3917 (1986).
47. Armit, P. W., Boyd, A. S. F., and Stephenson, T. A., *J. Chem. Soc., Dalton Trans.*, 1663 (1975).
48. Voelkel, R., *Angew. Chem.* **100**, 1525 (1988).
49. Sing, K. S. W., Everett, D. H., Haul, R. A. W., Moscou, L., Pierotti, R. A., Rouquérol, J., and Siemieniewska, T., *Pure and Appl. Chem.* **57**, 603 (1985).
50. Francis, A. W., *J. Phys. Chem.* **58**, 1099 (1954).
51. Bartle, K. D., Clifford, A. A., Jafar, S. A., and Shilstone, G. F., *J. Phys. Chem. Ref. Data* **20**, 728 (1991).
52. James, B. R., and Markham, L. D., *Inorg. Chem.* **13**, 97 (1974).
53. Lopez, T., Herrera, L., Gomez, R., Zou, W., Robinson, K., and Gonzalez, R. D., *J. Catal.* **136**, 621 (1992).
54. Schroth, W., Andersch, J., Schädler, H.-D., and Spitzner, R., *Chem. Ztg.* **113**, 261 (1989).
55. Leitner, W., Dinjus, E., and Gassner, F., *J. Organomet. Chem.* **475**, 257 (1994).
56. James, B. R., *Inorg. Chim. Acta*, 73 (1970).
57. Whittlesey, M. K., Perutz, R. N., and Moore, M. H., *Organometallics* **15**, 5166 (1996).
58. Graf, E., and Leitner, W., *J. Chem. Soc., Chem. Commun.*, 623 (1992).
59. Gassner, F., and Leitner, W., *J. Chem. Soc., Chem. Commun.*, 1465 (1993).